RSC Advances

PAPER

View Article Online
View Journal | View Issue

Cite this: *RSC Adv.*, 2019, **9**, 36011

A novel and fast responsive turn-on fluorescent probe for the highly selective detection of Cd^{2+} based on photo-induced electron transfer†

Meng-Xia Huang,[a] Cai-Hua Lv,[a] Qing-Da Huang,[a] Jia-Ping Lai *[a] and Hui Sun*[b]

Received 14th August 2019
Accepted 15th October 2019

DOI: 10.1039/c9ra06356k

rsc.li/rsc-advances

A novel, highly sensitive and fast responsive turn-on fluorescence probe, 2,2′-((1*E*,1′*E*)-((1,10-phenanthroline-2,9-diyl)bis(methanylylidene)) bis(azanylylidene)) diphenol (ADMPA), for Cd^{2+} was successfully developed based on 2,9-dimethyl-1,10-phenanthroline and *o*-aminophenol. ADMPA showed a remarkable fluorescence enhancement toward Cd^{2+} against other competing cations, owing to the suppression of the photo-induced electron transfer (PET) and CH=N isomerization. A good linear relationship (R^2 = 0.9960) was obtained between the emission intensity of ADMPA and the concentration of Cd^{2+} (0.25–2.5 μM) with a detection limit of 29.3 nM, which was much lower than that reported in literature. The binding stoichiometry between ADMPA and Cd^{2+} was 2 : 1 as confirmed by the Job's Plot method, which was further confirmed by a ^{1}H NMR titration experiment. Moreover, the ADMPA probe was successfully applied to detect Cd^{2+} in real water samples with a quick response time of only 6.6 s, which was about 3–40 times faster than the reported cadmium ion probe.

Introduction

Cadmium is a highly toxic heavy metal that has been classified as a category I human carcinogen by the International Agency for Research on Cancer (IARC).[1] Nowadays, cadmium contamination in the environment, as we all know, mainly comes from the emission from the industrial production of batteries, fertilizers, pigments, metallurgy and electroplates. In particular, in recent years, an increasing number of quantum dots containing cadmium have been synthesized and used widely in various laboratories. The pollution to the environment due to these quantum dots should not be neglected. However, the cadmium that enters the soil and water is absorbed by animals and plants, which can finally enter humans body through intake, thus posing a serious potential threat to human health.[2–4] Moreover, the long-term exposure to cadmium-containing environments for humans or animals not only impedes the normal deposition of calcium in the bones and causes osteoporosis, but also impairs the normal function of the immune, nervous, renal and reproductive systems.[5,6] Therefore, it is of great significance to develop a rapid and accurate method for the qualitative and quantitative detection of cadmium ions in environmental samples.

To date, the primary means for detecting cadmium ions are atomic absorption spectrometry (AAS),[7,8] inductively coupled plasma mass spectrometry (ICP-MS),[9,10] electrochemical methods[11–14] and microfluidic technologies.[15] These detection methods have the advantages of high sensitivity, low detection limit and wide linear range. However, these methods have high maintenance costs and complicated sample pretreatment methods. In this regard, a fluorescent probe/sensor is a promising alternative route for metal ion and anion detection due to their advantages of an excellent selectivity, high sensitivity, low cost, handy operation and biological compatibility compared with other detection methods. Therefore, the fluorescent probe/sensor has attracted increasing attention for its design and development.[16–22] Although cadmium ion fluorescent probes/sensors have been reported in literature,[23–28] there are still some difficulties that need to be overcome such as the complicated synthesis procedure, poor water solubility and slow response speed.

In the present work, a simply synthesized, highly sensitive and fast responsive turn-on fluorescence probe for Cd^{2+} based on a photo-induced electron transfer (PET) and CH=N isomerization was successfully synthesized. The fluorescence characterization of the obtained probe towards metal ions was investigated in detail. The synthetic probe exhibited an evident fluorescence enhancement and quick response to Cd^{2+}. Meanwhile, the binding stoichiometry and binding mechanism were also explored through the Job's Plot method, FT-IR characterization and ^{1}H NMR titration experiment.

[a]*School of Chemistry & Environment, South China Normal University, Guangzhou 510006, Guangdong, China. E-mail: laijp@scnu.edu.cn; Fax: +86-20-39310187; Tel: +86-20-39310257*

[b]*College of Environmental Science & Engineering, Guangzhou University, Guangzhou 510006, Guangdong, China. E-mail: cherrysunhui@aliyun.com*

† Electronic supplementary information (ESI) available. See DOI: 10.1039/c9ra06356k

Experimental section

Materials and apparatus

All reagents and solvents employed for the synthesis were purchased from commercial suppliers and used without further purification. ADMPA was dissolved in methanol at a concentration of 2 mM as a stock solution and stored in the refrigerator at 4 °C. All of the metal ions, including Ag^{+}, Al^{3+}, Ba^{2+}, Be^{2+}, Ca^{2+}, Cd^{2+}, Co^{2+}, Cr^{3+}, Cu^{2+}, Fe^{2+}, Fe^{3+}, Hg^{2+}, K^{+}, Mg^{2+}, Mn^{2+}, Ni^{2+}, Pb^{2+} and Zn^{2+} were in the chloride form or nitrate form. All the other reagents and solvents used in the synthesis and analysis were of analytical reagent grade and distilled water was used throughout the experiment.

^{1}H NMR and ^{13}C NMR experiments were conducted on a Varian AS 400 MHz NMR system in DMSO-d_6 with TMS as an internal standard. Elemental analyses for C, H and N were performed on a Vario EL III Organic Element Analyzer (Elementar, GER). The emission spectra were recorded on a FL-4600 spectrometer (Hitachi, Japan). The time-resolved fluorescence lifetime measurement was measured using a FLS920 transient fluorescence spectrometer (EI, UK). The FT-IR spectra were measured in the 4000–400 cm^{-1} range with KBr pellets on a Spectrum Two FT-IR spectrometer (PerkinElmer, USA). The mass spectral data for DMP-CHO was measured on a LCQ DECA XP MAX mass spectrometer (Thermo, USA).

Synthesis

Synthesis of 1,10-phenanthroline-2,9-dicarboxaldehyde (DMP-CHO). As shown in Scheme 1, 10-phenanthroline-2,9-dicarboxaldehyde (DMP-CHO) was synthesized *via* a mildly modified synthetic procedure that was previously reported.[29] Briefly, selenium dioxide (2.77 g, 0.025 mol) was dissolved in 75 mL of 1,4-dioxane and heated to reflux for 30 min. Afterwards, 2,9-dimethyl-1,10-phenanthroline (2.61 g, 0.012 mmol) in 1,4-dioxane (50 mL) was added dropwise into the flask and the reaction was stirred at 85 °C for 6 h. The solid–liquid mixture was subsequently filtered by diatomite while hot. A pale-yellow precipitate formed in the filtrate after cooling to ambient temperature. After removing the solvent, the obtained crude product was further purified by recrystallization in DMF and washed with hot water several times. Yield: 85%. ^{1}H NMR (400 MHz, DMSO-d_6): 10.32 (s, 2H), 8.77 (d, 2H), 8.27 (d, 2H), 8.25 (s, 2H). ESI-mass *m*/*z* calculated value for 237.06; experimental value was 237.05.

Synthesis of 2,2′-((1*E*,1′*E*)-((1,10-phenanthroline-2,9-diyl) bis(methanylylidene)) bis(azanylylidene))diphenol (ADMPA). ADMPA was synthesized based on a reported procedure[30] with a slight modification. Generally, 0.1180 g (0.5 mmol) of 1,10-phenanthroline-2,9-di-carbaldehyde and 10 mL of methanol were successively added into a 50 mL round-bottom flask. The mixture was stirred at room temperature for 30 min. Then, 0.1310 g (1.2 mmol) of an *o*-aminophenol methanol solution (15 mL) was slowly added dropwise into the flask. The solution started to become turbid 5 min later. The reaction process was monitored by TLC. The reaction was stopped when the spot for the raw material disappeared. After removing the solvent, an ADMPA yellow product was obtained and washed with methanol for three times. Yield: 85%. ^{1}H NMR (400 MHz, DMSO-d_6): δ (ppm) 9.29 (s, 2H), 9.13 (s, 2H), 8.80 (d, 2H), 8.65 (d, 2H), 8.13 (s, 2H), 7.46 (s, 2H), 7.17 (t, 2H), 6.97 (d, 2H), 6.91 (t, 2H). ^{13}C NMR (100 MHz, DMSO-d_6): δ (ppm) 159.58, 155.20, 152.27, 145.58, 137.47, 136.98, 130.05, 129.16, 128.15, 121.37, 120.43, 120.15, 116.96. Anal. calcd. for $C_{26}H_{18}N_4O_2$: C 74.63, H 4.34, N 13.39, found: C 74.26, H 3.96, N 13.68.

Fluorescence characterization

Procedures for fluorescence measurement. Firstly, 8.4 mg of ADMPA was dissolved in 10 mL of methanol to prepare a 2 mM

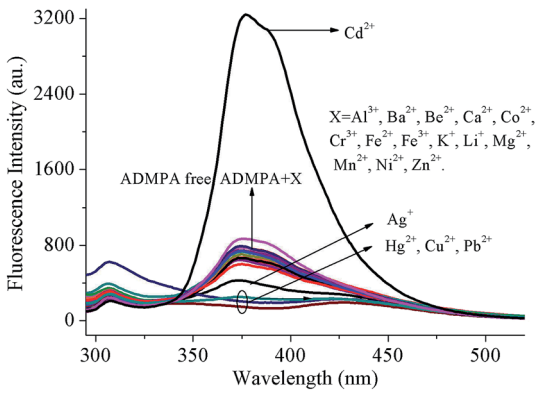

Fig. 1 Emission spectral changes for ADMPA (5 μM) induced by the addition of various metal ions (5 μM) in a DMF-water (v/v, 3 : 7) solution at room temperature.

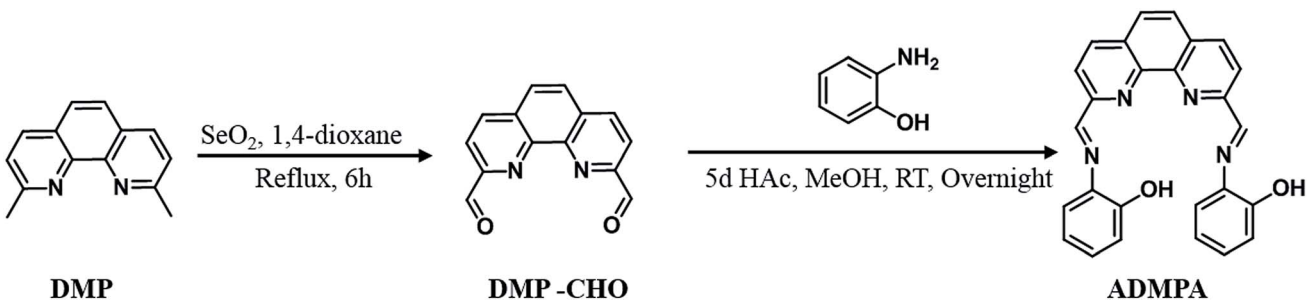

Scheme 1 The synthetic route for the ADMPA probe.

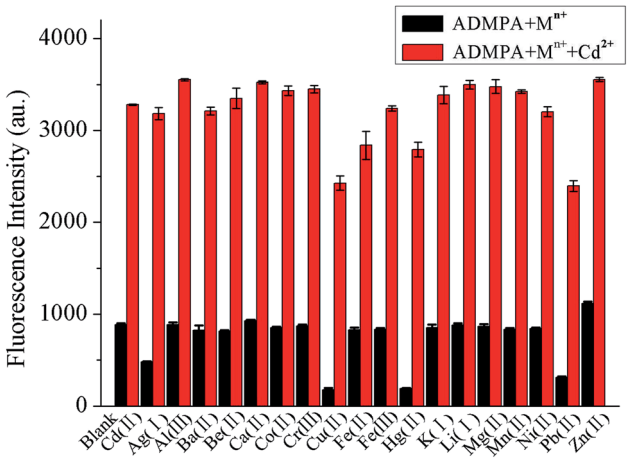

Fig. 2 The influence of single metal ions (10 μM) on the interaction between ADMPA (5 μM) and Cd^{2+} (5 μM) in a DMF-water (v/v, 3 : 7) solution.

ADMPA stock solution for subsequent use. The concentration of all the metal ion stock solutions was 10 mM. The test solution was obtained by adding 25 μL of the ADMPA stock solution and a fixed volume of each metal ion stock solution in a 10 mL disposable plastic centrifuge tube, and then diluting the solution to 10 mL *via* the addition of a DMF-water (v/v, 3 : 7) solution. After mixing the fluorescent probe with metal ions properly, the fluorescence spectra of ADMPA was obtained on a FL-4600 spectrometer at room temperature. The excitation wavelength of the fluorescence spectrometer was set at 275 nm. The λ_{ex} slit width was 2.5 nm, except for the quantitative determination experiments (5 nm). The λ_{em} slit width was 5 nm and the voltage was 700 V.

Job plot method. For the Job's plot measurement, ADMPA (2 mM) in methanol and Cd^{2+} (1 mM) in water were prepared. A series of test solutions that contained different mole ratios of Cd^{2+} and ADMPA were prepared and measured. The Job's plot was drawn by plotting *F versus* the mole fraction of Cd^{2+}, where *F* was the fluorescence intensity of each test solution at 377 nm.

FT-IR characterization

For the FT-IR characterization, ADMPA powder, cadmium nitrate powder and potassium bromide powder were thoroughly mixed and ground at a mass ratio of 1 : 0.5 : 100, 1 : 1 : 100, and 1 : 2 : 100. After grinding, these powders were dried in a vacuum oven at 50 °C overnight. Finally, ADMPA and the different mass ratios of ADMPA-Cd^{2+} were measured using a Spectrum Two FT-IR spectrometer (PerkinElmer, USA).

^{1}H NMR titration experiments

For the ^{1}H NMR titration experiments, 0, 0.25, 0.5 and 1.0 equiv. of Cd^{2+} were added into the ADMPA (4.18 mg, 0.01 mmol) DMSO-d_6 solution to obtain different mole fractions of the ADMPA-Cd^{2+} complex. Then, the ^{1}H NMR spectra of these solutions were recorded on a Varian 400 MHz NMR system.

Recovery investigation

Tap water, Yanhu water and Zhujiang River (Guangzhou, China) water were filtered with a 0.22 μm microporous membrane and then mixed with DMF at a volume ratio of 7 : 3. Owing to the low concentration level of Cd^{2+} in the real sample, the addition recovery method was adopted. The concentration of ADMPA and Cd^{2+} were fixed to 5 μM and 1 μM, respectively.

Results and discussion

Selectivity of the ADMPA probe towards Cd^{2+}

The selectivity of the fluorescent probe is very important for the selective determination of target analytes. For this purpose, the recognition ability of the ADMPA probe was investigated *via* the fluorescence characterization towards metal ions, including Ag^+, Al^{3+}, Ba^{2+}, Be^{2+}, Ca^{2+}, Cd^{2+}, Co^{2+}, Cr^{3+}, Cu^{2+}, Fe^{2+}, Fe^{3+}, Hg^{2+}, K^+, Mg^{2+}, Mn^{2+}, Ni^{2+}, Pb^{2+} and Zn^{2+}. As shown in Fig. 1, the ADMPA probe presented a fluorescence emission at 377 nm under an excitation wavelength of 275 nm. However, only Cd^{2+} ion produced a noticeable turn-on fluorescence response to ADMPA (Fig. 1, black line) when the same amount of ADMPA was added into above mentioned cations. This was attributed to the formation of a ADMPA-Cd^{2+} complex with a more rigid

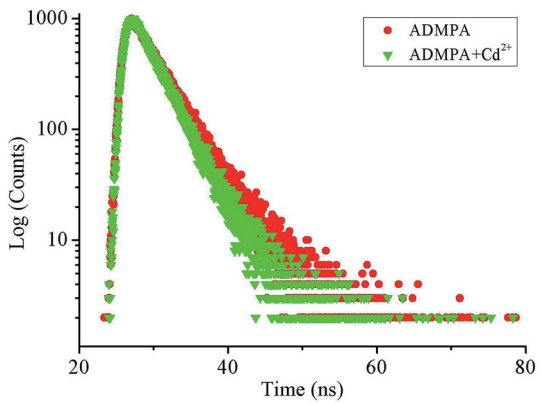

Fig. 3 Time-resolved fluorescence decay of ADMPA and ADMPA-Cd^{2+} in a DMF-water (v/v, 3 : 7) solution.

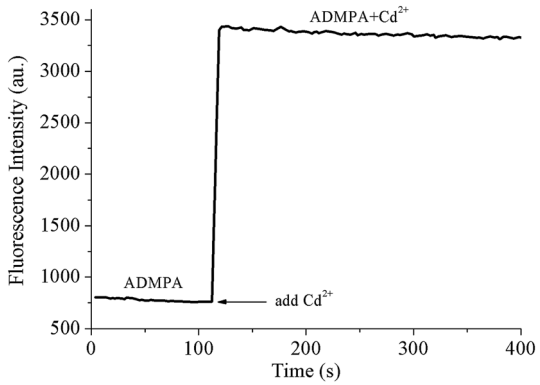

Fig. 4 On-line monitoring of the reaction velocity process for ADMPA (20 μM) and Cd^{2+} (20 μM) in a DMF-water (v/v, 3 : 7) solution.

Table 1 Comparison of the detection limit, detection media and response time for Cd^{2+} between the proposed method and those reported in literature

Probe	Solvent	$\lambda_{ex}/\lambda_{em}$	LOD (μM)	Response time	Ref.
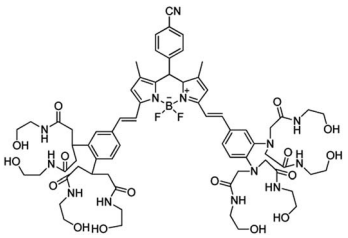	DMSO/Tris–HCl (1 : 9)	620/639	—	20 s	23
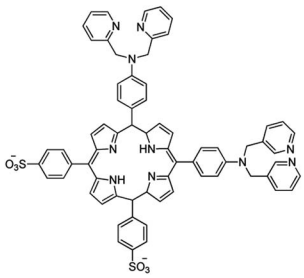	HEPES	418/611 653	0.032	4 min	24
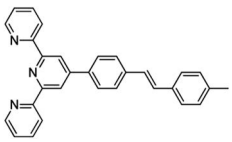	DMSO/H_2O (1 : 1)	341/473	0.314	—	25
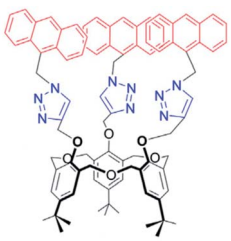	ACN	365/418	0.128	—	26
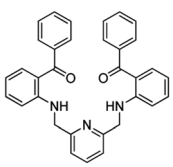	ACN/HEPES (1 : 5)	400/561	0.010	0.3 min	27
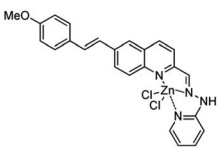	MeOH/H_2O (3 : 7)	400/485 560	—	—	33
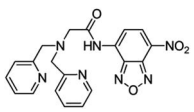	H_2O	460/567	0.01	—	34
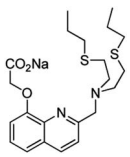	HEPES	315/419	0.60	—	35

Table 1 (*Contd.*)

Probe	Solvent	$\lambda_{ex}/\lambda_{em}$	LOD (μM)	Response time	Ref.
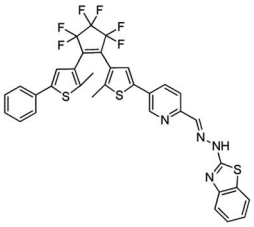	ACN	402/519	0.32	—	36
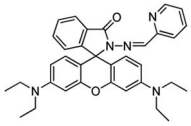	ACN/HEPES (2 : 8)	308/590	0.010	—	37
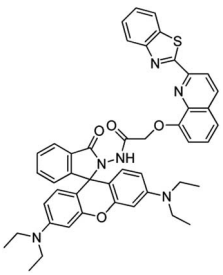	MeOH/H_2O (1 : 4)	360/470 585	0.27	—	38
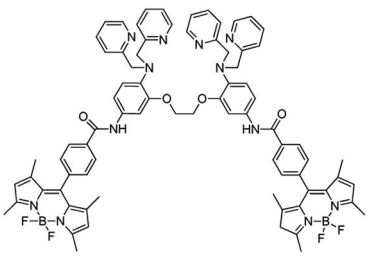	DMSO/HEPES (1 : 4)	460/511	0.077	—	39
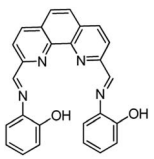	**DMF/H_2O (3 : 7)**	**275/377**	**0.029**	**6.6 s**	**This work**

conjugated structure, which hindered the rotation of CH=N and the suppression of the photo-induced electron transfer (PET) quenching process that resulted in the chelation-enhanced fluorescence (CHEF) effect.[31,32]

In order to investigate if the probe/sensor could be applied to detect target analytes in complicated environmental samples, the selectivity and anti-interference capability were critical factors used to evaluate the properties of the chemosensor. Thus, to further investigate the anti-interference capability of the ADMPA probe towards Cd^{2+} against 18 other competitive metal ions, binding competition experiments were performed. It can be seen from Fig. 2 that the fluorescence emission intensity changes for ADMPA in a DMF-water (v/v, 3 : 7) solution upon the addition of 2 equiv. of the other single metal ions (black bars). The results showed that most of the competing ions had no influence on the emission spectra of ADMPA apart from Cu^{2+} and Pb^{2+}, which produced a certain fluorescence quenching after continuous treatment with 1 equiv. of Cd^{2+}. This was attributed to the fact that Cu^{2+} and Pb^{2+} were in the same group of elements as Cd^{2+}, which possessed the same charge and a similar electronic layer structure. Nevertheless, the quenching degree of the fluorescence intensity at 377 nm was relatively acceptable when the 18 mixed metal ions were added into the ADMPA-Cd^{2+} complex (Fig. S5†). All of the above mentioned phenomena strongly certified that ADMPA could be used as a highly selective and sensitive fluorescent 'turn-on' chemosensor for Cd^{2+}.

The fluorescence lifetime of the fluorescent molecular probe was closely related to its own structure and the micro-environment of the fluorescent probe. Researchers can directly understand the changes in the studied system by measuring the time-resolved fluorescence spectrum. Herein,

the time-resolved fluorescence spectra of ADMPA and ADMPA-Cd^{2+} were measured. As shown in Fig. 3, the lifetime decays fit a single exponential decay profile with a lifetime of 3.78 ns ($\chi^2 = 1.031$) and 3.31 ns ($\chi^2 = 1.072$) for ADMPA and the ADMPA-Cd^{2+} complex, respectively, which were attributed to the inhibition of CH=N isomerization and the rearrangement of the charge rendered by the suppression of the photo-induced electron transfer (PET).

The response time for the probe towards the target is also an essential criteria for judging its performance, which determines whether it is suitable for on-site or/and on-line detection. Therefore, the response time for ADMPA towards Cd^{2+} was investigated by monitoring the fluorescence intensity change of ADMPA after the addition of Cd^{2+} on a FL-4600 fluorescence spectrophotometer. As shown in Fig. 4, it was clear that the fluorescence intensity of ADMPA sharply increased after the addition of an equal amount of Cd^{2+}. Then, the signal remained roughly unchanged. It is worthwhile to note that the quick response time of ADMPA towards Cd^{2+} was only 6.6 s, which was 3–40 times faster than the reported cadmium ion probe (Table 1). The fast response time allows for the possibility of the on-site or on-time detection of Cd^{2+}.

Quantitative determination of Cd^{2+}

The fluorescence sensing properties of ADMPA towards Cd^{2+} were also explored by fluorescence titration experiments in a DMF-water (v/v, 3 : 7) solution. As shown in Fig. 5, the fluorescence intensity of ADMPA (5 μM) at 377 nm gradually increased with the increase in the Cd^{2+} concentration. A good linear relationship ($R^2 = 0.9960$) between the fluorescence spectra of ADMPA (5 μM) and the Cd^{2+} concentration was obtained from 0.025 to 2.5 μM with a detection limit of 29.3 nM according to the equation, DL = 3SD/S, where SD is the standard deviation of ten times the blank measurements and S is the slope of the calibration curve. The detection limit of ADMPA towards Cd^{2+} in this work was much lower than most values reported in literature (Table 1). Furthermore, the response time of ADMPA towards Cd^{2+} (6.6 s) was also much faster than reported literature (Table 1). Finally, the ADMPA probe was applied for the detection of Cd^{2+} in tap water, lake water and Zhujiang River water. Satisfactory recoveries between 97.72% and 101.1% with a RSD ($n = 3$) under 4.8% were obtained, which suggested that the proposed method possessed a good accuracy (Table 2 and S2†).

Table 2 The recovery of Cd^{2+} in Tap water/Yanhu water/Zhujiang River water

Real sample	Added/μM	Detected/μM	Recovery/%	RSD/% ($n = 3$)
Tap water	1.0	1.004	100.4	3.7
Yanhu water	1.0	1.011	101.1	2.6
Zhujiang River water	1.0	0.9772	97.72	4.8

Binding affinity of ADMPA to Cd^{2+}

In order to explore the binding mode for the coordination of ADMPA and Cd^{2+}, a Job's plot analysis was performed. As shown

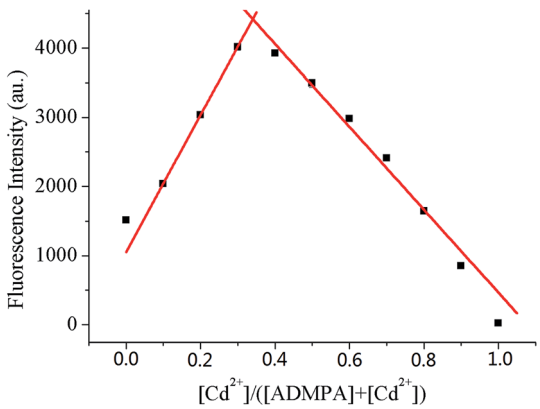

Fig. 6 Job's plot for determining the stoichiometry of ADMPA bound with Cd^{2+} in a DMF-water (v/v, 3 : 7) solution. The total concentration was 10 μM.

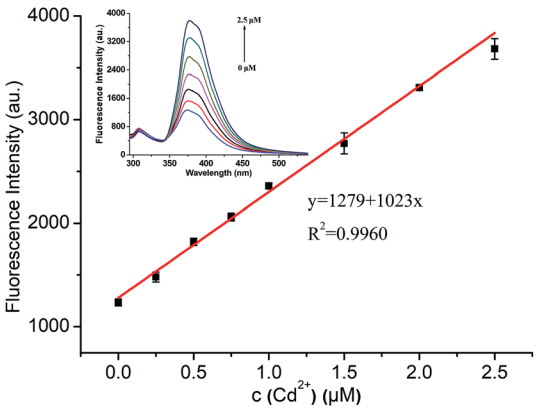

Fig. 5 The linear relationship between the fluorescence intensity of ADMPA and the concentration of Cd^{2+}. Inset: fluorescence wavelength scanning of the ADMPA solution (5 μM) upon the addition of various equivalents of Cd^{2+}.

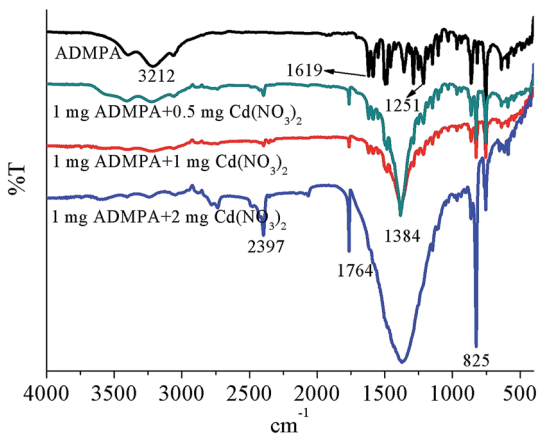

Fig. 7 FT-IR of ADMPA and the ADMPA-Cd^{2+} complex.

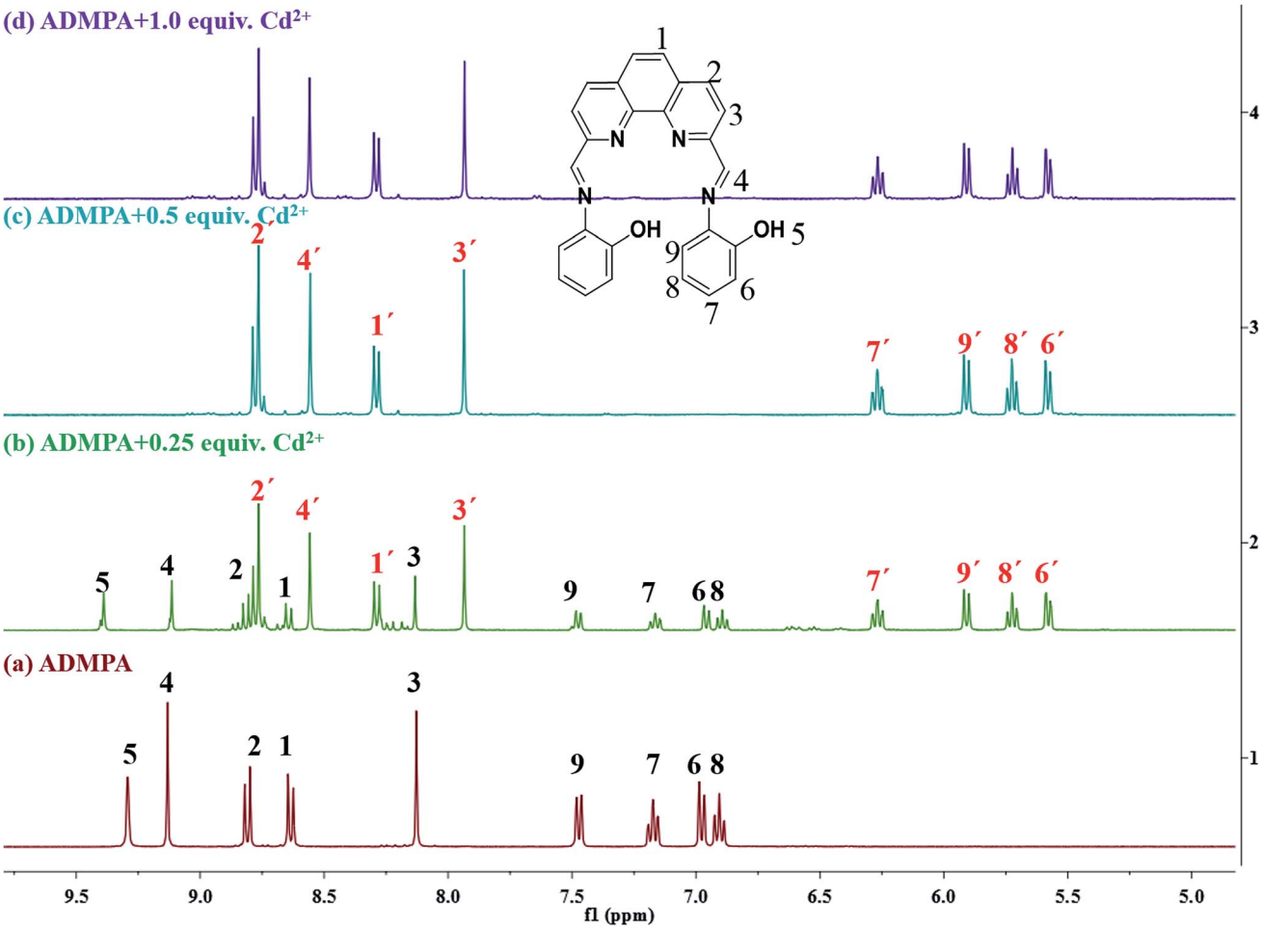

Fig. 8 ^{1}H NMR titration of ADMPA and ADMPA with Cd^{2+} (DMSO-d_6) for (a) ADMPA only, (b) ADMPA with 0.25 equiv. of Cd^{2+}, (c) ADMPA with 0.5 equiv. of Cd^{2+} and (d) ADMPA with 1.0 equiv. of Cd^{2+}.

in Fig. 6, it was clear that the fluorescence intensity reached a maximum value when the molar ratio of $[Cd^{2+}]/[Cd^{2+}]$ + [ADMPA] was about 0.33. This clearly suggested that the ratio of ADMPA bound with Cd^{2+} was 2 : 1. The binding constant (K_a) for the ADMPA-Cd^{2+} complex was calculated with fluorescence titration spectra from Fig. 5 using a revised Benesi–Hildebrand equation:[40,41] $I_0/I - I_0 = (a/b - a)(1/K_a[C] + 1)$, where I_0 and I are the fluorescence intensities of ADMPA at 377 nm in the absence and existence of Cd^{2+}, respectively, a and b are constants, K_a is the association constant and $[C]$ is the concentration of Cd^{2+}.[42] The calculated binding constant was 3.15×10^5 M^{-1} from the plot of $1/(I - I_0)$ against $1/[C]$ for Cd^{2+}.

To further elucidate the mechanism for the binding modes between the ADMPA probe and Cd^{2+}, FT-IR titration experiments for ADMPA towards $Cd(NO_3)_2$ were also performed. The infrared spectra for the ADMPA probe and different mass ratios of the ADMPA-$Cd(NO_3)_2$ complex were obtained. As shown in Fig. 7, there were apparent changes in the IR spectra between free ADMPA and ADMPA-$Cd(NO_3)_2$. Three distinct peaks for ADMPA at 3212 cm^{-1}, 1619 cm^{-1} and 1251 cm^{-1} represented a O–H vibration, CH=N vibration and C–O vibration, respectively. Those peaks gradually disappeared in the spectrum of ADMPA-$Cd(NO_3)_2$ with the increase in the $Cd(NO_3)_2$ mass. Meanwhile, new peaks at 2397 cm^{-1}, 1764 cm^{-1}, 1383 cm^{-1} and 825 cm^{-1} appeared. Among them, the peak at 1764 cm^{-1} was obviously the stretching vibration peak of C=O and the other three peaks were the characteristic peaks of CO_2, NO_3^- and NO_2^-, respectively. These changes clearly implied that the phenolic hydroxyl and imine may have been involved in the

Table 3 ^{1}H NMR shifts for ADMPA and ADMPA with Cd^{2+}

H atom	ADMPA	ADMPA + Cd^{2+} (mole ratio 2 : 1)	Downfield shift
H_1	8.62	8.30	0.32
H_2	8.80	8.76	0.04
H_3	8.13	7.93	0.20
H_4	9.13	8.56	0.57
H_5	9.29	Disappear	—
H_6	6.97	5.59	1.38
H_7	7.17	6.27	0.90
H_8	6.91	5.72	1.19
H_9	7.46	5.92	1.54

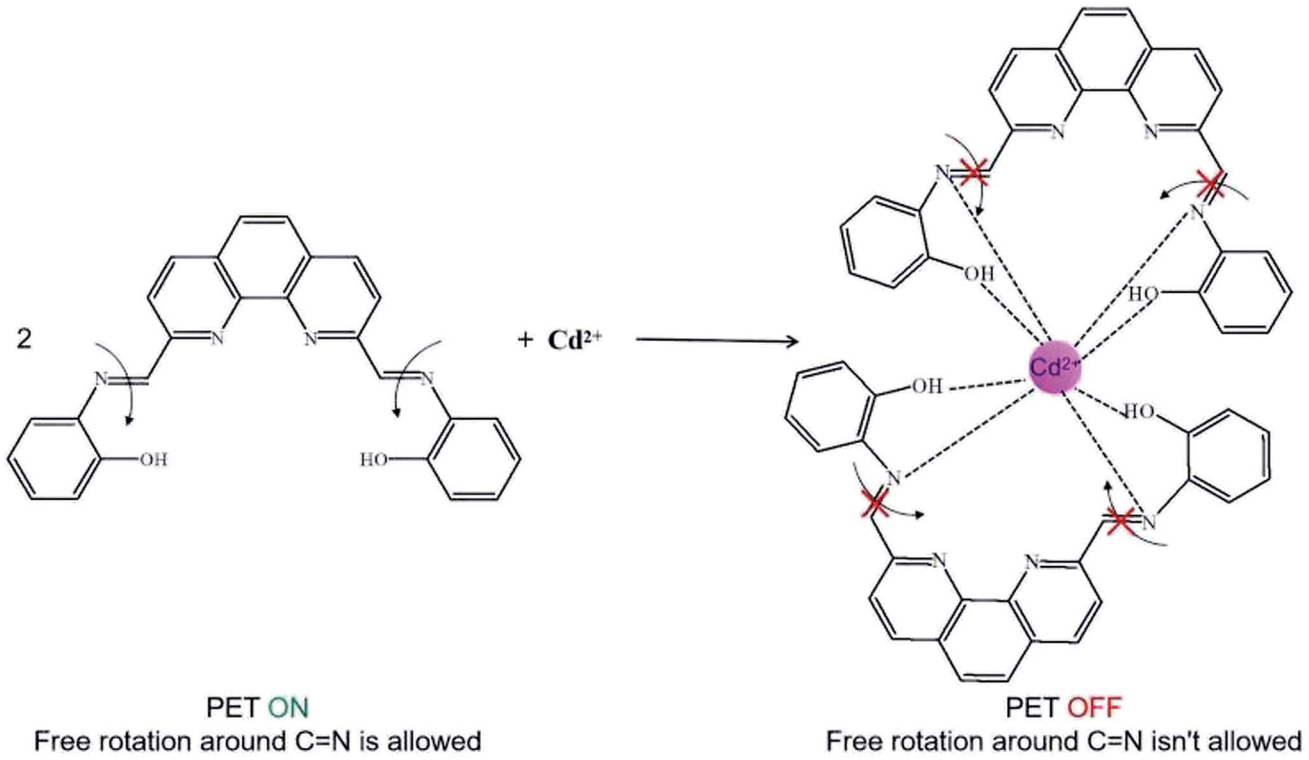

Fig. 9 Proposed binding mode for ADMPA with Cd^{2+}.

complex reaction between ADMPA and Cd^{2+}. Owing to the electron transfer from ADMPA to Cd^{2+}, the double bond in C=O was formed and the fluorescence was enhanced.

For a better understanding, ^1H NMR titration experiments were performed by adding various amounts of Cd^{2+} to ADMPA in DMSO-d_6. As shown in Fig. 8, the peak for OH_5 at 9.29 ppm gradually disappeared with the increase of Cd^{2+}, while the signal for other hydrogen atoms at a different downfield shift changed from 0.04 ppm to 1.54 ppm (Table 3). These changes suggested that OH_5 participated in the coordination of ADMPA towards Cd^{2+} and the formation of the complex changed the conjugated structure of ADMPA, causing a shift in the hydrogen atoms of the benzene ring and phenanthroline skeleton.

Based on the above results, a possible binding mode for ADMPA towards Cd^{2+} was proposed, as shown in Fig. 9. In the absence of Cd^{2+}, the nitrogen atom of imine transferred an electron to the phenanthroline ring (PET ON) and the C=N group could rotate freely. When Cd^{2+} was added, the phenolic hydroxyl and neighboring imine nitrogen reacted with Cd^{2+}, resulting in the restriction of the PET process and C=N isomerisation. Meanwhile, there was a full rearrangement in the charge distribution of the entire molecule, which increased the rigidity and turned the fluorescence on.

Conclusions

In conclusion, a highly-sensitive and fast responsive turn-on fluorescence ADMPA probe for Cd^{2+} detection was successfully developed based on 2,9-dimethyl- 1,10-phenanthroline and *o*-aminophenol. The binding mode of ADMPA and Cd^{2+} was confirmed by a Job's plot analysis and ^1H NMR titration experiments with a ratio of 2 : 1. The obtained ADMPA probe was applied for the detection of Cd^{2+} at a concentration as low as 29.3 nM in DMF-water. The proposed method was applied to detect Cd^{2+} in an actual sample with a satisfactory recovery. More importantly, the excellent response velocity provided a possibility for the real-time detection of Cd^{2+}. Thus, the proposed method could be a promising alternative route for Cd^{2+} detection in environmental samples.

Conflicts of interest

There are no conflicts to declare.

Acknowledgements

This work was supported and sponsored by the National Natural Science Foundation of China (21677053 and 21876033).

References

1 M. Taki, M. Desaki, A. Ojida, S. Iyoshi, T. Hirayama, I. Hamachi and Y. Yamamoto, *J. Am. Chem. Soc.*, 2008, **130**(38), 12564–12565.
2 M. J. Mclaughlin and B. R. Singh, *Cadmium in Soils and Plants*. Springer Netherlands, 1999.

3 S. Satarug, J. R. Baker, S. Urbenjapol, M. Haswell-Elkins, P. E. B. Reilly, D. J. Williams and M. R. Moore, *Toxicol. Lett.*, 2003, **137**(1–2), 65–83.
4 S. Clemens, *Biochimie*, 2006, **88**(11), 1707–1719.
5 L. Strumylaite, A. Kontrimaviciute, R. Kregzdyte and S. Ryselis, *Epidemiology*, 2003, **14**(5), S54.
6 X. Huo, C. W. Gu and X. Xu, *J. Neurotrauma*, 2008, **25**(7), 881.
7 Z. Nazari, M. A. Taher and H. Fazelirad, *RSC Adv.*, 2017, **7**(71), 44890–44895.
8 M. Sadeghi, E. Rostami, D. Kordestani, H. Veisi and M. Shamsipur, *RSC Adv.*, 2017, **7**(44), 27656–27667.
9 J. White, A. Celik, R. Washington, V. Yilmaz, T. Mitchum and Z. Arslan, *Microchem. J.*, 2018, **139**, 242–249.
10 E. Begu, B. Snell and Z. Arslan, *Microchem. J.*, 2019, **145**, 412–418.
11 X. Y. Zheng, S. Chen, J. B. Chen, Y. H. Guo, J. Peng, X. C. Zhou, R. X. Lv, J. D. Lin and R. Y. Lin, *RSC Adv.*, 2018, **8**(14), 7883–7891.
12 J. Z. Huang, S. L. Bai, G. Q. Yue, W. X. Cheng and L. S. Wang, *RSC Adv.*, 2017, **7**(45), 28556–28563.
13 D. F. Qin, A. R. Chen, X. Mamat, Y. T. Li, X. Hu, P. Wang, H. Cheng, Y. M. Dong and G. Z. Hu, *Anal. Chim. Acta*, 2019, **1078**, 32–41.
14 Y. S. Fang, B. Cui, J. Z. Huang and L. S. Wang, *Sens. Actuators, B*, 2019, **284**, 414–420.
15 M. Kim, J. W. Lim, H. J. Kim, S. K. Lee, S. J. Lee and T. Kim, *Biosens. Bioelectron.*, 2015, **65**, 257–264.
16 S. Ellairaja, R. Manikandan, M. T. Vijayan, S. Rajagopal and V. S. Vasantha, *RSC Adv.*, 2015, **5**(78), 63287–63295.
17 Q. Yang, J. H. Li, X. Y. Wang, H. L. Peng, H. Xiong and L. X. Chen, *Biosens. Bioelectron.*, 2018, **112**, 54–71.
18 P. A. Gale and C. Caltagirone, *Coord. Chem. Rev.*, 2018, **354**, 2–27.
19 L. Li, L. F. Liao, Y. P. Ding and H. Y. Zeng, *RSC Adv.*, 2017, **7**(17), 10361–10368.
20 J. S. Wu, W. M. Liu, J. C. Ge, H. Y. Zhang and P. Wang, *Chem. Soc. Rev.*, 2011, **40**(7), 3483–3495.
21 H. N. Kim, W. X. Ren, J. S. Kim and J. Yoon, *Chem. Soc. Rev.*, 2012, **41**(8), 3210–3244.
22 D. Wu, A. C. Sedgwick, T. Gunnlaugsson, E. U. Akkaya, J. Yoon and T. D. James, *Chem. Soc. Rev.*, 2017, **46**(23), 7105–7123.
23 T. Y. Cheng, T. Wang, W. P. Zhu, X. L. Chen, Y. J. Yang, Y. F. Xu and X. H. Qin, *Org. Lett.*, 2011, **13**(14), 3656–3659.
24 W. B. Huang, W. Gu, H. X. Huang, J. B. Wang, W. X. Shen, Y. Y. Lv and J. Shen, *Dyes Pigm.*, 2017, **143**, 427–435.
25 A. Sil, A. Maity, D. Giri and S. K. Patra, *Sens. Actuators, B*, 2016, **226**, 403–411.
26 X. K. Jiang, Y. Ikejiri, C. C. Jin, C. Wu, J. L. Zhao, X. L. Ni, X. Zeng, C. Redshaw and T. Yamato, *Tetrahedron*, 2016, **72**(32), 4854–4858.
27 S. Chithiraikumar, C. Balakrishnan and M. A. Neelakantan, *Sens. Actuators, B*, 2017, **249**, 235–245.
28 S. S. Zehra, R. A. Khan, A. Alsalme and S. Tabassum, *J. Fluoresc.*, 2019, **29**(4), 1029–1037.
29 S. D. Gupta, B. Revathi, G. I. Mazaira, M. D. Galigniana, C. V. S. Subrahmanyam, N. L. Gowrishankar and N. M. Raghavendra, *Bioorg. Chem.*, 2015, **59**, 97–105.
30 S. Ameerunisha and P. S. Zacharias, *Polyhedron*, 1994, **13**(15–16), 2327–2332.
31 T. Sun, Q. F. Niu, Y. Li, T. D. Li and H. X. Liu, *Sens. Actuators, B*, 2017, **248**, 24–34.
32 X. L. Yue, Z. Q. Wang, C. R. Li and Z. Y. Yang, *Tetrahedron Lett.*, 2017, **58**(48), 4532–4537.
33 W. P. Ye, S. X. Wang, X. M. Meng, Y. Feng, H. T. Sheng, Z. L. Shao, M. Z. Zhu and Q. X. Guo, *Dyes Pigm.*, 2014, **101**(1), 30–37.
34 Y. Liu, Q. Qiao, M. Zhao, W. T. Yin, L. Miao, L. Q. Wang and Z. C. Xu, *Dyes Pigm.*, 2016, **133**, 339–344.
35 X. J. Jiang, Y. Fu, H. Tang, S. Q. Zang, H. W. Hou, T. C. W. Mak and H. Y. Zhang, *Sens. Actuators, B*, 2014, **190**(1), 844–850.
36 D. B. Zhang, S. Y. Li, R. M. Lu, G. Liu and S. Z. Pu, *Dyes Pigm.*, 2017, **146**, 305–315.
37 M. Maniyazagan, R. Mariadasse, J. Jeyakanthan, N. K. Lokanath, S. Naveen, K. Premkumar, P. Muthuraja, P. Manisankar and T. Stalin, *Sens. Actuators, B*, 2017, **238**, 565–577.
38 K. Aich, S. Goswami, S. Das, C. Das Mukhopadhyay, C. K. Quah and H. K. Fun, *Inorg. Chem.*, 2015, **54**(15), 7309–7315.
39 S. B. Maity, S. Banerjee, K. Sunwoo, J. S. Kim and P. K. Bharadwaj, *Inorg. Chem.*, 2015, **54**(8), 3929–3936.
40 P. Madhu and P. Sivakumar, *J. Mol. Struct.*, 2019, **1185**, 410–415.
41 P. Ravichandiran, A. Boguszewska-Czubara, M. Masłyk, A. P. Bella, P. M. Johnson, S. A. Subramaniyan, K. S. Shim and D. J. Yoo, *Dyes Pigm.*, 2020, **172**, 107828.
42 R. Dwivedi, D. P. Singh, B. S. Chauhan, S. Srikrishna, A. K. Panday, L. H. Choudhury and V. P. Singh, *Sens. Actuators, B*, 2018, **258**, 881–894.